Analytical and numerical modelling of air-trapping during wetting of unsaturated soils

Author 1*

- Riccardo Scarfone, PhD, Geotechnical Engineer
- Geotechnical Consulting Group, London, United Kingdom. Formerly: James Watt School of Engineering, University of Glasgow, Glasgow, United Kingdom
- https://orcid.org/0000-0003-0268-9537
- r.scarfone@gcg.co.uk

***Corresponding author.**

Author 2

- Simon J. Wheeler*, Cormack Professor of Civil Engineering
- James Watt School of Engineering, University of Glasgow, Glasgow, United Kingdom
- https://orcid.org/0000-0003-1493-2434
- Simon.Wheeler@glasgow.ac.uk

Abstract
At high values of degree of saturation, the apparent soil water retention curve (SWRC) measured in a wetting test in the laboratory may differ from the true SWRC, because of the occurrence of air trapping, meaning that gas pressure in the trapped air is greater than the externally applied gas pressure. Physical arguments indicate that the true SWRC will reach full saturation at a positive value of suction. Analytical and numerical modelling of the phenomenon of gas trapping during wetting shows that, once air trapping occurs, the apparent SWRC depends upon many aspects of the wetting test conditions and is not a fundamental representation of the soil behaviour. The only correct way to represent the occurrence and influence of air trapping during wetting within numerical modelling of boundary value problems is to use the true SWRC in combination with a gas conductivity expression that goes to zero at the air-discontinuity point.

Declarations

Conflicts of interest/Competing interests. The authors have no conflicts of interest to declare that are relevant to the content of this article.

Availability of data and material. All data presented in this article will be made available upon acceptance of the paper in a repository online in accordance with funder data retention policies. The online repository will be the institutional repository "Enlighten" of the University of Glasgow.

Code availability. The software used for the analyses Code_Bright is publicly available for download.

Authors' contributions. Riccardo Scarfone: Conceptualization, Methodology, Formal analysis and investigation, Writing - original draft preparation, Resources. Simon J. Wheeler: Conceptualization, Methodology, Writing - review and editing, Resources, Supervision.

Acknowledgements

1. Introduction

Full saturation is often not achieved for an unsaturated soil subjected to wetting, because of the phenomenon of air trapping (Stonestrom and Rubin, 1989). As described by Peck (1960), Poulovassilis (1970) and Stonestrom and Rubin (1989), air trapping affects the measured soil water retention curve (SWRC), which relates the degree of liquid saturation S_l to the suction s (the difference between pore-gas pressure p_g and pore-liquid pressure p_l). The occurrence of air trapping means that, during a wetting process, an unsaturated soil may not reach full saturation even though the applied suction becomes zero.

During a wetting process, the liquid phase (typically water) enters the smaller pores of the soil first and subsequently the larger pores, and the gas phase (typically air) is consequently expelled. In order for the gas to flow out of the soil during wetting, the gas phase must form continuous gas flow channels or dissolve into the liquid and then move by diffusion, which is a relatively slow process. When high values of degree of saturation are attained, larger pores filled with gas may however be entirely surrounded by smaller pores filled with liquid, so that the passageways for gas flow become blocked (Stonestrom and Rubin 1989). At this point, termed the air-discontinuity point by Scarfone et al. (2020), the gas conductivity becomes zero, because the gas phase is discontinuous (Fischer et al., 1997). From this point, further decreases in the suction applied to the boundary of a soil sample result in an increase in the gas pressure in the trapped bulbs of air. In this situation, the only way for gas to continue to be expelled is through the very slow processes of dissolution of air within the liquid phase and then diffusion of dissolved air within the liquid phase (Williams, 1966; Mahmoodi and Gallant, 2021). Diffusion of the dissolved air is driven by a gradient in the dissolved air concentration between the liquid phase around the trapped air bulbs (higher concentration) and the liquid phase adjacent to continuous air voids or adjacent to an external atmospheric boundary (lower concentration).

Several SWRC models that attempt to include the effects of air trapping have been proposed. Most of them (e.g. Kool and Parker, 1987; van Geel and Sykes, 1997; Chen et al., 2015; Beriozkin and Mualem, 2018) involve wetting curves which do not reach full saturation even when suction is reduced to zero. In others (e.g. Chen et al., 2019), wetting curves reach saturation only by

31 applying cycles of wetting and drying in the negative suction range, i.e. positive liquid pressure

32 relative to gas pressure. Although these seem sensible and pragmatic approaches, these wetting

33 SWRCs are not a fundamental representation of the soil behaviour, because they are based on

34 use of an apparent suction s_{ext}, which is the suction imposed or monitored at the external

35 boundary of a soil sample. However, once the air becomes trapped, the pore-gas pressure p_g in

36 the trapped air bulbs is greater than the gas pressure $p_{g,ext}$ imposed at the boundary of the sample

37 (unless the very slow process of diffusion of dissolved air has finished) and the true suction s

38 internally within the soil is therefore higher than s_{ext}.

39

40 As discussed, the occurrence of air trapping is strictly related to the gas phase becoming

41 discontinuous during wetting at the air-discontinuity point. In some fields of geoscience, such as

42 the petroleum engineering field, it is common practise to model the gas conductivity vanishing at

43 a value of liquid degree of saturation lower than 1 (e.g. Killough, 1976). However, this approach

44 for gas conductivity has generally been combined with SWRCs which do not reach full saturation

45 at s=0 in order to capture the effect of air trapping, as discussed above. In the field of geotechnical

46 engineering, the gas conductivity is often unrealistically modelled to vanish only at full saturation,

47 even in problems in which the phenomenon of air trapping is specifically intended to be

48 represented (e.g. Chen and Wei, 2016).

49

50 The apparent SWRC, of S_l plotted against s_{ext}, is not a property of the material, because it is also

51 affected by various aspects of the wetting conditions, such as the degree of saturation at the start

52 of wetting (Sharma and Mohamed, 2003) and the precise time-history of the variation of s_{ext}

53 applied or recorded at the boundary (Hannes et al., 2016). In contrast, physical arguments

54 suggest that, for a main wetting curve, the true SWRC, of S_l plotted against the true suction s

55 internally within the soil (based on the gas pressure within the trapped air bulbs), is a fundamental

56 property of the soil (at least for a non-deformable soil).

57

58 Physical arguments also suggest that, provided hydrophobic soils are excluded, the true SWRC

59 will reach full saturation at a positive value of s. The arguments run as follows. Firstly, if, when

60 the externally applied suction is zero ($s_{ext} = 0$ and hence $p_{g,ext} = p_l$), trapped air temporarily exists

61 within a soil sample, then the curvature of the gas-liquid interfaces (and the constraints imposed

62 by satisfying the contact angle condition if an interface comes into contact with a soil particle)

63 would mean that the gas pressure p_g within trapped air bulbs would be higher than the pore-liquid

64 pressure p_l, irrespective of whether a trapped air bulb entirely filled a soil void (so that gas-liquid

65 interfaces come into contact with surrounding soil particles) or was sufficiently small to form an

66 occluded bubble entirely surrounded by water. This means that p_g would be greater than $p_{g,ext}$ and

67 this pressure difference would drive dissolution of air from the trapped air bulb and subsequent

68 diffusion of dissolved air to the external boundary. This diffusion of dissolved air would only cease

69 once the trapped air had completely disappeared. Hence, with an externally applied suction of

70 zero, the only possible final state after diffusion of dissolved air has finished (representing the true

71 SWRC) is a fully saturated condition. In fact, further consideration of this logic suggests that the

72 true SWRC for a non-hydrophobic soil should reach full saturation at a positive value of suction

73 corresponding to the pressure difference across a spherical gas-liquid interface corresponding to

74 the largest sphere that could fit within the largest voids of the soil.

75

76 Correct theoretical interpretation and modelling of the phenomenon of air trapping are relevant to

77 various applications in the field of geotechnical engineering. These include, for example, the

78 interpretation and modelling of laboratory wetting tests (e.g. Chen et al, 2019) and the modelling

79 of rainfall propagation into the ground with subsequent effects on the water table (e.g. Fayer and

80 Hillel 1986a,b). Recently, the introduction of the "induced partial saturation" technique (Yegian et

81 al, 2007; Mahmoodi and Gallant, 2021), consisting of the deliberate introduction of gas into the

82 ground eventually becoming trapped for mitigation of liquefaction risks, also led to the need of a

83 correct representation of the phenomenon of air trapping.

84

85 The first aim of this paper is to demonstrate the significance of air-trapping through a simple

86 analytical model representing wetting of an infinitesimally small soil element and to show the

87 corresponding differences between the apparent SWRC and the true SWRC for this idealized

88 situation. The second aim is to show, through numerical modelling of realistic wetting tests on soil

89 samples of finite size, that the apparent SWRC, of S_l plotted against s_{ext}, is not a fundamental

90 property of the soil and to demonstrate how various aspects of the wetting test conditions will

91   influence this apparent SWRC. The third and final aim is to show that correct representation of

92   the influence of air trapping during wetting within numerical modelling of boundary value problems

93   can only be achieved by using the true SWRC in combination with an unsaturated gas conductivity

94   expression that goes to zero at the air-discontinuity point.

95

96   **2. Analytical model of wetting of an infinitesimal element**

97   *2.1 Analytical model*

98   An analytical model for the wetting of an infinitesimally small element of soil is considered first, to

99   demonstrate the potential impact of air trapping on the apparent SWRC. The analysis of an

100   infinitesimal element will lay the basis for the subsequent interpretation of the numerical analyses

101   undertaken for a finite size element. The approach taken is to calculate the apparent SWRC, of

102   S_l plotted against s_{ext}, of a given soil with a particular true SWRC, of S_l plotted against the true

103   internal suction s within the soil, to demonstrate how the apparent SWRC differs from the true

104   SWRC. In the interests of simplicity, the soil element is assumed to be incompressible. The

105   analytical model was developed with and without consideration of diffusion of dissolved air within

106   the liquid phase. Results from the case without diffusion of dissolved air are useful for developing

107   understanding of some of the phenomena involved and for subsequent interpretation of the results

108   of the numerical modelling of finite sized samples, where diffusion of dissolved air is typically

109   incomplete (in the infinitesimal element, if dissolved air diffusion is included, the diffusion

110   completes instantaneously).

111

112   Liquid flow rate q_l and gas flow rate q_g through unit area are respectively proportional to the

113   hydraulic gradient ∇h_l and gradient of gas head ∇h_g by means of Darcy's law, i.e. $q_l = k_l \cdot \nabla h_l$ and

114    $q_g = k_g \cdot \nabla h_g$, where k_l and k_g are the liquid conductivity and gas conductivity respectively,

115    $h_l = z + p_l/\gamma_l$ and $h_g = z + p_g/\gamma_g$, with z, γ_l and γ_g being respectively the elevation above a datum level,

116   the unit weight of liquid and the unit weight of gas. In an infinitesimally small element, non-

117   equilibrated distributions of p_l and p_g mean that $\nabla h_l \rightarrow \infty$ and $\nabla h_g \rightarrow \infty$, because the element size

118   tends to zero. As a consequence, liquid flow through an infinitesimal element under non-

119   equilibrated distribution of p_l would be $q_l \rightarrow \infty$ and thus equilibration of pore-liquid pressure

120   distribution occurs instantaneously. This means that the pore-liquid pressure within the interior of

4

121   the element p_l can be considered always identical to the liquid pressure $p_{l,ext}$ applied at the

122   boundary. Regarding the gas flow from the interior of the element to the boundary under non-

123   equilibrated distribution of p_g, this is $q_g \rightarrow \infty$ if the degree of saturation S_l of the element is less than

124   the degree of saturation at the air-discontinuity point $S_{l,AD}$ because the gas phase is continuous

125   within the element ($k_g > 0$). In this case, equilibration of pore-gas pressure occurs instantaneously

126   and hence the pore-gas pressure within the interior of the element p_g can be considered identical

127   to the gas pressure imposed at the boundary $p_{g,ext}$. However, once the degree of saturation attains

128   or exceeds the air-discontinuity value $S_{l,AD}$, gas flow between the element interior and the

129   boundary is no longer possible ($q_g = 0$ because $k_g = 0$), meaning that p_g and $p_{g,ext}$ can take different

130   values in the absence of diffusion of dissolved air within the liquid phase.

131

132   For an infinitesimal element (in which $p_l = p_{l,ext}$), the true internal suction s and the externally applied

133   suction s_{ext} are defined as:

134    $s = p_g - p_l$

135   1.

136    $s_{ext} = p_{g,ext} - p_{l,ext} = p_{g,ext} - p_l$

137   2.

138   For values of S_l below $S_{l,AD}$, p_g and $p_{g,ext}$ are identical, hence s and s_{ext} are identical and the

139   apparent SWRC ($S_l : s_{ext}$) is the same as the true SWRC ($S_l : s$). However, for values of S_l above

140    $S_{l,AD}$, p_g and $p_{g,ext}$ differ in the absence of diffusion, hence s and s_{ext} are not the same and the

141   apparent SWRC is different to the true SWRC.

142

143   Taking into account diffusion, a non-equilibrated distribution of gas pressure in an infinitesimal

144   element would induce an infinite gradient of dissolved air concentration within the liquid. As the

145   diffusive flux of dissolved air is proportional to the gradient of dissolved air concentration,

146   according to Fick's law, a non-equilibrated distribution of gas pressure within the infinitesimal

147   element would lead to an infinite diffusive flux, meaning that the internal pore gas pressure would

148   equilibrate instantaneously with the external gas pressure. Therefore, the true SWRC coincides

149   with the apparent SWRC, even for values of S_l greater than $S_{l,AD}$ (i.e. even in the range where air

150   trapping occurs), for an infinitesimal element in which diffusion is included.

151

152 In order to evaluate the apparent SWRC of an infinitesimal element in the absence of diffusion,

153 two possible cases are considered here which differ for the type of wetting occurrence:

154   i)   the gas pressure imposed at the element boundary $p_{g,ext}$ is held constant and the

155   external pore-liquid pressure $p_{l,ext}$ is gradually increased from a negative value

156   relative to $p_{g,ext}$, i.e. the principle of a negative column SWRC test (Haines, 1930);

157   ii)   the liquid pressure imposed at the element boundary $p_{l,ext}$ is held constant and the

158   external pore-gas pressure $p_{g,ext}$ is gradually decreased from a positive value relative

159   to $p_{l,ext.}$, i.e. axis translation technique (Hilf, 1956) used for example in the pressure

160   plate apparatus (Richards and Fireman, 1943).

161

162 *2.1.1 Case i) ($p_{g,ext}$ held constant and $p_{l,ext}$ gradually increased)*

163 The value of p_g within the trapped air bulbs is equal to $p_{g,ext}$ at the air-discontinuity point ($S_l = S_{l,AD}$,

164 $s = s_{AD}$) where air trapping commences during wetting. Beyond this point, the value of p_g within

165 the trapped air bulbs increases and it can be related to further increases of S_l by applying the

166 ideal gas law to the fixed mass of gas within the trapped air bulbs (given that diffusion of dissolved

167 air from the trapped air bulbs is excluded):

168 $$p_g = p_{g,ext} \frac{1 - S_{l,AD}}{1 - S_l} = p_{g,ext} + p_{g,ext} \frac{S_l - S_{l,AD}}{1 - S_l}$$

169 3.

170 where $p_{g,ext}$ is a constant in Eq.3. p_g and $p_{g,ext}$ are expressed as absolute pressures in Eq.3 and

171 hereafter and hence, from Eqs. 1 and 2, p_l is also expressed as an absolute pressure. Eq. 3

172 assumes no change in the total volume of soil voids within the element (i.e. the soil is assumed

173 to be incompressible) and constant temperature. As a consequence of Eq.3, comparing Eqs. 1

174 and 2 gives:

175 $$s = s_{ext} + p_{g,ext} \frac{S_l - S_{l,AD}}{1 - S_l}$$

176 4.

177 or:

178 $$s_{ext} = s - p_{g,ext} \frac{S_l - S_{l,AD}}{1 - S_l}$$

6

179   5.

180

Given a soil with a particular true SWRC, the procedure to determine the apparent SWRC for

182   Case i), for values of s_{ext} below the air-discontinuity point (s_{AD}, $S_{l,AD}$), where air trapping

183   commences, is as follows:

184   • Consider a value of true internal suction s slightly lower than the air-discontinuity value

185   s_{AD} and calculate the corresponding value of degree of saturation S_l from the equation of

186   the true SWRC.

187   • Insert the values of s and S_l in Eq. 5 to calculate the corresponding value of externally

188   applied suction s_{ext}. The value of S_l and the value of s_{ext} now provide the coordinates of

189   a point on the apparent SWRC.

190   Repeat the process for gradually decreasing values of s to determine the complete curve of S_l

191   plotted against s_{ext}, defining the apparent SWRC.

192

193   *2.1.2 Case ii) ($p_{l,ext}=p_l$ held constant and $p_{g,ext}$ gradually decreasing)*

194   At the air-discontinuity point ($S_l = S_{l,AD}$, $s = s_{AD}$) where air trapping commences during wetting, the

195   value of p_g within the trapped air bulbs is equal to $p_{l,ext} + s_{AD}$. Beyond this point, with diffusion of

196   dissolved gas excluded, by applying the ideal gas law (similar to Eq. 3), the value of p_g within the

197   trapped air bulbs can be related to further variation of S_l as follows:

198   $$p_g = \left(p_{l,ext} + s_{AD}\right) \cdot \frac{1 - S_{l,AD}}{1 - S_l}$$

199   6.

200   where $p_{l,ext}$ is a constant in Eq.6. As a consequence of Eq. 6, Eq. 1 gives:

201   $$s = p_g - p_{l,ext} = \frac{\left(p_{l,ext} + s_{AD}\right) \cdot \left(1 - S_{l,AD}\right)}{1 - S_l} - p_{l,ext}$$

202   7.

203   Postulating that $S_l > S_{l,AD}$, Eq. 7 leads to $s > s_{AD}$, but this solution is impossible because the true

204   SWRC monotonically increases with decreasing suction. On the other hand, postulating that $S_l <$

205   $S_{l,AD}$, Eq. 7 leads to $s < s_{AD}$, but this solution is again impossible for the same reason. Thus, the

206   only possible solution of Eq. 7 is: $s = s_{AD}$ and $S_l = S_{l,AD}$. This means that, if diffusion of dissolved

207   air is excluded and wetting occurs by maintaining a constant liquid pressure and gradually

208   decreasing the pore gas pressure applied at the boundary, once air trapping commences, the

209   internal pore liquid pressure, pore gas pressure, suction and degree of saturation remain constant

210   and equal to the values attained at the air-discontinuity point. Hence, the apparent SWRC for

211   Case ii) for values of s_{ext} below s_{AD}, where air trapping commences, consists of a constant value

212   of S_l, equal to $S_{l,AD}$.

213

214   ***2.2 Analytical results***

215   Figure 1 shows the SWRCs obtained using the analytical model described above for two

216   infinitesimal soil specimens: one representative of a sand and one representative of a clay. For

217   each soil, three SWRCs are compared:

218   -   the true SWRC (continuous line), which coincides with the SWRC of an infinitesimal

219   element in the presence of diffusion of dissolved air;

220   -   the apparent SWRC obtained by varying $p_{l,ext}$ and holding $p_{g,ext}$ constant and equal to

221   atmospheric pressure p_{at} = 100 kPa (dashed line), in the absence of diffusion;

222   -   the apparent SWRC obtained by varying $p_{g,ext}$ and holding $p_{l,ext}$ constant and equal to

223   atmospheric pressure p_{at} = 100 kPa (dotted line), in the absence of diffusion.

224   The true SWRC was modelled using the van Genuchten (1980) model, with the van Genuchten

225   expression and the parameter values for the two soils given in the first section of Table 1. For

226   both soils, the van Genuchten parameter S_{ls}, giving the maximum value of degree of saturation

227   on the true SWRC, was selected as S_{ls} = 1. This means that the true SWRCs in Figure 1 tend to

228   a fully saturated condition as s tends to zero. The choice of the value of the air-discontinuity

229   degree of saturation, where air trapping commences, was based on typical values found in the

230   literature (Pham et al., 2005; Likos et al., 2013). In particular, based on several laboratory SWRC

231   tests on different soil types, Likos et al. (2013) showed that the ratio between the volumetric water

232   content at the end of a main wetting process and that at full saturation is on average 0.85, typically

233   varying in the range of 0.85 ± 0.1 (corresponding to a relative standard deviation of 12%). For

234   both soils shown in Figure 1, the value of the air-discontinuity degree of saturation was taken as

235     $S_{l,AD}$ = 0.85. Hence, for both sand and clay, the apparent SWRC in the absence of diffusion

236   diverges from the true SWRC at $S_l = S_{l,AD}$ = 0.85 in Figure 1. This occurs at s_{AD} = 1.90 kPa for the

237   sand and s_{AD} = 185 kPa for the clay.

238

239 Figure 1 shows that, for both soils, the apparent SWRCs (in the absence of diffusion) are

240 significantly different from the true SWRCs, with S_l reaching a maximum value significantly less

241 than 1 as s_{ext} is reduced towards zero, demonstrating the influence of air trapping. Inspection of

242 Figure 1 also shows that the effect of air trapping is noticeably different for the sand and the clay.

243 The apparent SWRC obtained by varying $p_{l,ext}$ (i.e. $p_{g,ext}$ = 100 kPa) is almost horizontal for $s_{ext} <$

244 s_{AD} for the sand, whereas it shows noticeable increase of S_l for $s_{ext} < s_{AD}$ for the clay. This is

245 because the compression of the trapped air, as p_g increases above $p_{g,ext} = p_{at}$, is very small in the

246 case of the sand and more significant in the case of the clay. In the case of the sand, $p_g = p_{at} =$

247 100 kPa (as an absolute pressure) at the point where air trapping commences ($s = s_{ext} = s_{AD} =$

248 1.90 kPa) and p_g = 101.88 kPa (s = 1.88 kPa) at the end of wetting when s_{ext} = 0. This increase

249 of p_g, from 100kPa to 101.88kPa, causes only a very small amount of compression of the trapped

250 air. In contrast, for the clay, p_g increases from $p_g = p_{at}$ = 100 kPa at the onset of air trapping (at s

251 = $s_{ext} = s_{AD}$ = 185 kPa) to p_g = 195 kPa at the end of wetting when s_{ext} = 0, and this increase of p_g

252 is sufficient to cause significant compression of the trapped air.

253

254 The apparent SWRCs obtained by varying $p_{g,ext}$ (i.e. $p_{l,ext}$ = constant) are horizontal for both the

255 sand and the clay when $s_{ext} < s_{AD}$. In this case, when air is trapped, further decrease of the external

256 gas pressure $p_{g,ext}$ does not affect the internal gas pressure p_g. This means that the gas volume

257 cannot vary and S_l remains equal to $S_{l,AD}$.

258

259 **3. Numerical modelling of wetting tests on samples of finite size**

260 *3.1 Numerical model*

261 Numerical modelling of wetting tests on soil samples of finite size was performed to provide more

262 realistic simulations of the impact of air trapping and to investigate how various aspects of wetting

263 test conditions would influence the apparent SWRC. Multi-physics numerical modelling was

264 performed with the Code_Bright finite element software (Olivella et al., 1996). Advective liquid

265 and gas flows (governed by Darcy's law) were included in all analyses, whereas diffusion of

266 dissolved air within the liquid phase (governed by Fick's law) was included in some analyses but

267 not in others, in order to assess its influence. Diffusion of water vapour within the gas phase was

9

268   not included, because it would always be insignificant compared to liquid water flow at the high

269   values of S_l occurring in the simulations (Scarfone, 2020). The concentration of dissolved air in

270   the liquid phase was governed by Henry's law and the density of the gas phase was governed by

271   the law of ideal gases. Isothermal conditions were assumed. Although soils (in particular fine-

272   grained soils) deform as a result of wetting (or drying) processes, in the interest of simplicity the

273   soil was assumed to be non-deformable, but this assumption is not expected to affect qualitatively

274   the key findings presented in this paper. The various constitutive laws employed within the

275   numerical modelling are set out in full in Table 1.

276

277   The numerical simulations represented one-dimensional wetting tests performed on soil samples

278   of height 20 mm, which was within the range of sizes typically adopted in laboratory SWRC tests.

279   Two numerical models were considered, as shown in Figure 2. For both models, the external

280   pore-liquid pressure was controlled at the bottom boundary, which was impermeable to gas flow,

281   whereas the external pore gas pressure was controlled at the top boundary, which was

282   impermeable to liquid flow. For some simulations (see Figure 2a), the external pore-liquid

283   pressure was held constant at $p_{l,ext}$ = 100 kPa, i.e. equal to atmospheric pressure, while wetting

284   of the sample was induced by decreasing the external gas pressure $p_{g,ext}$ (e.g. the conditions of a

285   pressure plate apparatus). For comparison, another set of simulations was considered (Figure

286   2b), where the external pore-gas pressure was held constant $p_{g,ext}$ = 100 kPa while wetting of the

287   sample was induced by increasing the external liquid pressure $p_{l,ext}$ (e.g. the conditions of a

288   negative column SWRC apparatus). The influence of the mode of suction application was

289   assessed by comparing the results of these two set of analyses.

290

291   Simulations were performed with two different soils: one representative of a sand and the other

292   representative of a clay. Constitutive parameter values used for the two soils are given in Table

293   1. The true SWRC for each soil was represented again by the van Genuchten (1980) model and

294   the function for the relative liquid conductivity k_{rl} (giving the decrease of liquid conductivity with

295   decreasing degree of liquid saturation S_l) was given by the Mualem (1976) model. The relative

296   gas conductivity k_{rg} (giving the decrease of gas conductivity with decreasing degree of gas

297   saturation S_g, where $S_g = 1 - S_l$) was given by the following expression (Brooks and Corey, 1964)

298   implemented in Code_Bright:

299

$$k_{rg} = A \left(\frac{S_g - S_{rg}}{S_{gs} - S_{rg}} \right)^n$$

300

301   8.

302

303   For both soils, the values of A and S_{gs} in Eq. 8 were taken as $A = 1$ and $S_{gs} = 1$ and the value of

304   the exponent n was taken as 10/3 (Millington and Quirk, 1961). Eq. 8 predicts that the gas

305   conductivity falls to zero when the degree of gas saturation S_g decreases to a value S_{rg}. The

306   parameter S_{rg} therefore represents the degree of gas saturation at which the gas phase becomes

307   discontinuous, which corresponds to $S_{rg} = 1 - S_{l,AD}$. $S_{rg} = 0.15$ was assumed for both soils,

308   corresponding to $S_{l,AD} = 0.85$, in agreement with average values found in the literature (Likos et

309   al., 2013). Relative liquid and gas conductivity curves for the sand and the clay are shown in

310   Figure 3.

311

312   Figure 4 shows the variation with time of the suction s_{ext} applied at the boundaries of the models

313   either by decreasing $p_{g,ext}$ at the top boundary while maintaining $p_{l,ext}$ constant at the bottom

314   boundary, or by increasing $p_{l,ext}$ at the bottom boundary while maintaining $p_{g,ext}$ constant at the top

315   boundary, as discussed above. s_{ext} was controlled in a stepwise fashion, so that its value reduced

316   in a series of decrements. Each value of s_{ext} was applied for a fixed interval of time, namely 2

317   hours for the sand (see Figure 4a) and 600 hours for the clay (see Figure 4b). These time intervals

318   were selected as sufficient to allow complete equalization of pore-liquid pressure p_l throughout

319   the soil sample (see later) and were considered representative of what might be used in practice

320   for laboratory determination of SWRCs for samples of sands and clays respectively.

321

322   Figure 4 shows that, for each of the two soils, the specific values of externally applied suction s_{ext}

323   followed two different sequences, in different simulations. For the sand, for path 1, the initial value

324   of s_{ext} was 6 kPa and the subsequent values of s_{ext} were 2 kPa, 0.6 kPa and 0.2 kPa before a final

325   step to s_{ext} = 0, whereas for path 2 the initial value of s_{ext} was 10 kPa and the subsequent values

326   were 3 kPa, 1 kPa and 0.3 kPa, before a final step to s_{ext} = 0 (see Figure 4a). Similarly, for the

327   clay, for path 1 the initial value of s_{ext} was 600 kPa and the subsequent values of s_{ext} were 200

328   kPa, 60 kPa and 20 kPa before a final step to s_{ext} = 0, whereas for path 2 the initial value of s_{ext}

329   was 1000 kPa and the subsequent values were 300 kPa, 100 kPa and 30 kPa, before a final step

330   to s_{ext} = 0 (see Figure 4b). For both path 1 and path 2 and for both sand and clay, the values of

331   s_{ext} after the first decrement were above the air-discontinuity value s_{AD}, whereas all subsequent

332   values of s_{ext} were below s_{AD}. The intention of using paths 1 and 2 was to investigate the effect of

333   the precise sequence of values of externally applied suction s_{ext} on the apparent SWRC.

334

335   The validity of the numerical models, including the adopted mesh, was verified by some

336   preliminary numerical tests (Scarfone, 2020).

337

338   *3.2 Apparent SWRC*

339   Figure 5 shows the results of the numerical simulations on the sand (Figure 5a) and the clay

340   (Figure 5b), for the case where $p_{g,ext}$ was decreased at the top boundary while maintaining $p_{l,ext}$

341   constant at the bottom boundary (see Figure 2a). Figure 5 shows the apparent SWRC that would

342   be determined from the wetting test represented as the average degree of liquid saturation of the

343   soil sample $\overline{S_l}$ at the end of each 2 hour (sand) or 600 hour (clay) time interval plotted against the

344   value of externally applied suction s_{ext}. For each soil, results from 4 different numerical simulations

345   are presented, corresponding to path 1 and path 2, each with diffusion of dissolved air included

346   or excluded. The insets within Figure 5a and Figure 5b show the results of the final stages of the

347   numerical simulations with s_{ext} plotted on a linear scale, rather than the logarithmic scale of the

348   main figure, allowing the inclusion of results for the final wetting stage to s_{ext} = 0. Also shown in

349   Figure 5 for each soil is the true SWRC (the smooth continuous curve), which also represents the

350   apparent SWRC for an infinitesimally small element when diffusion of dissolved gas is included.

351   Finally, the apparent SWRC from the analytical model of the infinitesimally small element when

352   diffusion of dissolved air is excluded is shown by the smooth dashed curve.

353

354   Inspection of the numerical modelling results for the sand in Figure 5a shows very different results

355   for path 1 and path 2, whereas inclusion or exclusion of diffusion of dissolved air made very little

356   difference. For path 1 and path 2, the apparent SWRC of $\bar{S}_l$ plotted against s_{ext} in Figure 5a is

357   almost horizontal from the value of s_{ext} applied immediately before s_{ext} was first reduced below

358   the air-discontinuity value of suction $s_{AD} = 1.9$ kPa. For example, with path 2, the apparent SWRC

359   is almost horizontal from the point $s_{ext} = 3$ kPa, because the next decrement of s_{ext} was to $s_{ext} = 1$

360   kPa, which was less than s_{AD}. Air trapping within the soil sample occurred almost immediately

361   after s_{ext} was reduced below s_{AD}, because a thin zone of soil with $s < s_{AD}$, and hence with

362   discontinuous gas phase and gas conductivity equal to zero, was formed immediately at the top

363   boundary of the soil sample, preventing any subsequent flow of gas from the remainder of the

364   sample (even though in the majority of the sample s remained greater than s_{AD} and hence S_l

365   remained less than $S_{l,AD}$). The behaviour shown in Figure 5a means that the final average value

366   of degree of saturation $\bar{S}_l$ in a sand sample of finite size wetted to $s_{ext} = 0$ may be substantially

367   less than the local value of degree of saturation at which air trapping occurs at that location $S_{l,AD}$.

368   Also, the fact that the results of the numerical simulations shown in Figure 5a are very different

369   for paths 1 and 2 clearly means that, for sand samples, the apparent SWRC is highly dependent

370   on the precise sequence of values of applied suction s_{ext}.

371

372   Figure 5b shows that, for the clay samples, inclusion or exclusion of diffusion of dissolved air

373   made more difference to the results than it did for the sand samples. In particular, the effect of

374   diffusion for the clay samples was such that the internal pore-gas pressure almost equalised with

375   the applied external gas pressure at the end of each step, meaning that the apparent SWRCs

376   were almost coincident with the true SWRC and the influence of trapped air was thus negligible.

377

378   In the absence of air diffusion, for both sand and clay samples, $\bar{S}_l$ remains constant after air

379   trapping commences because further decreases in $p_{g,ext}$ do not induce variation of the internal

380   gas pressure and thus gas compression, as identified previously from consideration of an

381   infinitesimal element.

382

383 The results shown in Figure 6, unlike those shown in Figure 5, were obtained by varying $p_{l,ext}$ at

384 the bottom boundary and maintaining $p_{g,ext}$ constant at the top boundary equal to atmospheric

385 pressure 100 kPa (see Figure 2b). The results obtained for sand (Figure 6a) for this type of suction

386 application were similar to those shown in Figure 5a. By contrast, the results obtained in this case

387 for the clay sample (Figure 6b) show a different pattern from those shown previously in Figure 5b,

388 at least for the cases where diffusion of dissolved air is excluded. Figure 6b shows that, for the

389 numerical simulations of the clay samples, the value of $\overline{S}_l$ increased substantially as the wetting

390 test progressed beyond the point where air trapping commenced, even when air diffusion was

391 excluded. As discussed previously for the infinitesimal element, the significant increase of $\overline{S}_l$ after

392 air trapping commenced, even in the absence of diffusion, was a consequence of the compression

393 of the trapped air, caused by a substantial increase of gas pressure within the trapped air, induced

394 by the increase of external liquid pressure $p_{l,ext}$. In addition, inspection of Figure 6b shows that,

395 when air diffusion is excluded, the relatively small difference between the results for path 1 and

396 path 2 for the clay samples is attributable to the significant increase of $\overline{S}_l$ after air trapping

397 commences due to gas compression (so that it matters less where the apparent SWRC diverges

398 from the true SWRC).

399

400 With air diffusion excluded, once air trapping commenced in the sand sample, $\overline{S}_l$ showed very

401 little further increase (see Figure 6a), because subsequent increases of gas pressure p_g in the

402 trapped air were so small that they caused only very small amounts of compression of this trapped

403 air (similar to the infinitesimally small sand sample discussed previously). Figure 6a also shows

404 that inclusion of air diffusion had negligible impact on the apparent SWRC for the sand sample

405 (similar to Figure 5a).

406

407 A significant and original aspect of the results of the numerical analyses shown in Figures 5 and

408 6 worth highlighting is that the phenomenon of air trapping occurring during wetting was captured

409 by modelling the hydraulic behaviour of the materials with a SWRC attaining full saturation as

410 suction was reduced towards zero, in conjunction with a gas conductivity becoming zero at a

411 degree of gas saturation greater than zero.

412

413   *3.3 Gas and liquid pressures*

414   Figure 7 shows the variation of pore-gas pressure p_g and pore-liquid pressure p_l predicted in the

415   numerical simulations of the sand samples (Figures 7a and 7b) and the clay samples (Figures 7c

416   and 7d), with the applied time-histories of s_{ext} given by path 2, induced by varying $p_{g,ext}$ and

417   maintaining $p_{l,ext}$ = 100 kPa (i.e. the simulations for path 2 previously presented in Figure 5). Within

418   Figure 7, values of p_g and p_l are shown for points A and B (see Figure 2a), where the former was

419   at the bottom boundary of the numerical model ($p_{l,ext}$ = 100 kPa and q_g = 0) and the latter was at

420   the top boundary ($p_{g,ext}$ varying and q_l = 0). Results of the simulations with diffusion of dissolved

421   air either included or excluded are shown.

422

423   Although it is the pore-gas pressure that is controlled at the top boundary (point B), applied

424   changes in $p_{g,ext}$ also induced variation of p_l at this point. The values of p_l at point B in the sand

425   sample (Figure 7b) and in the clay sample (Figure 7d) show that the time intervals used for each

426   wetting stage (2 hours for the sand and 600 hours for the clay) were more than sufficient to ensure

427   equalisation of liquid pressure p_l throughout the samples, which occurred relatively quickly

428   because the high values of S_l implied high values of relative liquid conductivity k_{rl}.

429

430   Inspection of Figures 7a and 7c shows that in the first time interval (0-2h for sand, 0-600h for

431   clay), no air trapping occurred because s_{ext} was greater than s_{AD}, and p_g at point A therefore

432   equalised relatively quickly with the applied $p_{g,ext}$ at point B (see Figures 7a and 7c). Trapped air

433   was formed in the subsequent time intervals (>2h for sand, >600h for clay), when s_{ext} was less

434   than s_{AD}. Without diffusion, for both sand and clay, p_g at point A could not equalise with $p_{g,ext}$

435   imposed at point B because the air was trapped by a thin zone at the top of the sample with a gas

436   conductivity of zero (see below for full explanation). Even introducing the effect of diffusion, no

437   dissipation of excess gas pressure for the sand (Figure 7a) seemed to occur within the time of

438   the test. By contrast, the effect of diffusion for the clay (Figure 7b) was such that the excess gas

439   pressure at point A was almost fully dissipated within each time interval of 600h. The effect of

440   diffusion was thus negligible for the sand but crucial for the clay. The excess values of p_g within

441   the sand sample at the end of each wetting stage explains why the apparent SWRCs were

442   different from the true SWRC (see Figure 5a) whereas the almost complete equalisation of pore-

443 gas pressure throughout the clay sample explains why the apparent SWRCs almost coincided

444 with the true SWRC in the presence of diffusion (see Figure 5b).

445

446 In the sand sample (Figures 7a and 7b), at the beginning of the second time interval (starting at

447 a time of 2h), the applied change in $p_{g,ext}$ at point B also induced an almost instantaneous

448 reduction of p_l at point B, which quickly equalised with $p_{l,ext}$ applied at point A (see the inserts in

449 Figures 7a and 7b, showing the response between t = 2h and t = 2.005h). At the same time, p_g at

450 point A slightly decreased and quickly increased again although the externally applied suction

451 was $s_{ext} < s_{AD}$, i.e. the gas phase was expected to be trapped and no variations of p_g within the

452 sample were expected. This phenomenon can be explained by inspecting the profiles shown in

453 Figure 8 of p_g, p_l, s and S_l along the sand sample height. Profiles at two different times are shown:

454 t = 2.0002h (approx. 2 hours and 1 second), i.e. immediately after s_{ext} was decreased to 1 kPa,

455 corresponding to the minima of p_g at point A and p_l at point B shown respectively in Figures 7a

456 and 7b; and t = 2.1233h (approx. 2 hours and 7 minutes), i.e. when no further changes of p_l and

457 p_g were observed for the remainder of this wetting stage. Immediately after application of the step

458 change of $p_{g,ext}$ at point B (t = 2.0002h), p_g at the top boundary was equal to the externally applied

459 value $p_{g,ext}$ and it continuously increased towards the bottom. At the same time, the reduction in

460 $p_{g,ext}$ applied at the top boundary induced also a reduction of p_l at the top, and p_l increased

461 monotonically towards the bottom where it was equalised with the externally applied value $p_{l,ext}$ =

462 100 kPa. As a result, suction values at t = 2.0002h were between 2.5 and 3 kPa throughout the

463 entire sample, i.e. the suction values within the sample were higher than both the externally

464 applied suction s_{ext} and the air discontinuity value s_{AD}, even at the top boundary. This means that

465 the gas phase was not trapped at this time. After a short time interval (see t = 2.1233h) excess p_l

466 values dissipated and the p_l profile became uniform within the specimen, in equilibrium with $p_{l,ext}$

467 = 100 kPa. This means that, at the top of the sample (point B) where p_g remained equal to $p_{g,ext}$,

468 suction equalised with s_{ext} and it was thus lower than s_{AD}. In other words, a thin layer of

469 discontinuous gas phase formed at the top boundary of the specimen. As a consequence, the

470 gas phase became trapped within the specimen and did not form continuous pathways with the

471 exterior, meaning that the p_g profile in the remainder of the specimen did not equalise with $p_{g,ext}$

472   applied at the top boundary. Within the sample, excluding very close to the top boundary, the gas

473   phase was however continuous and the p_g profile therefore became uniform.

474

475   It should be highlighted that, although in the second time interval starting at t=2h the externally

476   applied suction was lower than the air-discontinuity value, meaning that no gas continuity might

477   be expected, some gas outflow from the specimen occurred at the beginning of this time interval.

478   As discussed above, this was the consequence of the fact that the gas phase was continuous

479   across the top boundary at the beginning of the time interval (e.g. see profiles at t = 2.0002h in

480   Figure 8). This means that the internal excess gas pressure slightly dissipated before the gas

481   phase became trapped at the top boundary.

482

483   In the case in which s_{ext} was varied by varying $p_{g,ext}$ and maintaining $p_{l,ext}$ = 100 kPa (i.e. the

484   simulations previously presented in Figure 6), trapped air was again formed when s_{ext} was less

485   than s_{AD} (>2h for sand, >600h for clay). At these time intervals, the applied increase of $p_{l,ext}$ at the

486   bottom (point A) caused an instantaneous increase of p_g at the same point. The pore-liquid

487   pressure p_l within the sample and at the top boundary quickly equalised with the value applied at

488   the bottom $p_{l,ext}$. As a consequence, the suction at the top boundary, where $p_{g,ext}$ = 100 kPa,

489   quickly equalised with s_{ext}, which was less than s_{AD}. Therefore, similar to what was observed in

490   Figures 7 and 8, a thin layer of discontinuous gas phase formed at the top boundary of the

491   specimen and hence the gas phase became trapped within the specimen and did not form

492   continuous pathways with the exterior. Equalisation of p_l along the specimen was so quick that

493   no significant dissipation of excess gas pressure occurred before the thin layer of discontinuous

494   gas phase formed at the top boundary.

495

496   ### 3.4 Factors influencing diffusion of dissolved air

497   Diffusion of dissolved air had greater influence on the wetting tests on clay (Figures 5b and 6b)

498   than on the wetting tests on sand (Figures 5a and 6a). This can be attributed to two different

499   factors. Firstly, in the wetting tests on clay, each value of s_{ext} was maintained for 600 hours,

500   compared to only 2 hours for the wetting tests on sand, meaning that there was simply more time

501   for diffusion of dissolved air in the tests on clay. Secondly, the values of excess gas pressure

502 within the trapped air, which drive the diffusion of dissolved air, were always less than 3 kPa

503 during the tests on sand (compare the values of p_g at points B and A in Figure 7a), whereas the

504 values of excess gas pressure within the trapped air immediately after each step change of s_{ext}

505 were substantially greater during the tests on clay (see Figure 7c). This second factor would

506 suggest that, after air trapping commenced, diffusion of dissolved air would dissipate excess pore-

507 gas pressure more quickly in tests on clay than in tests on sand. Additional numerical simulations

508 were performed to investigate the relative importance of these two factors.

509

510 Figure 9 shows the results of numerical simulations of wetting tests on sand for path 2 with each

511 value of s_{ext} maintained for either 2 hours (the original simulations shown in Figure 5a) or 600

512 hours (a new set of simulations). With each wetting stage lasting 600 hours, Figure 9 shows that

513 diffusion of dissolved air had a noticeable impact on the apparent SWRC, whereas there was

514 negligible impact of diffusion of dissolved air when each wetting stage lasted only 2 hours.

515 However, even with each wetting stage lasting 600 hours, the influence of diffusion of dissolved

516 air during the tests on sand (Figure 9) was still much less than in the tests on clay (Figure 5b).

517 This means that the higher values of excess gas pressure within the trapped air during tests on

518 clay are of considerable importance, in reducing the time required for dissipation of excess gas

519 pressures in trapped air by diffusion of dissolved air.

520

521 The fact that, after air trapping commences, dissipation of excess gas pressures by diffusion of

522 dissolved air occurs more slowly in tests on sands than during tests on clays means that, counter

523 to normal practice, after air trapping commences (at high values of S_l), wetting tests on sand

524 samples should be performed more slowly than wetting tests on clay samples if full equalization

525 of both p_l and p_g throughout the sample is to be achieved. This is, of course, in contrast to the

526 situation at lower values of S_l, when the gas phase is continuous, where it is tests on clay samples

527 that need to be performed slowest, because of the lower values of liquid conductivity for clays.

528 This very long persistence of trapped air in sand samples has been also confirmed by various

529 numerical (Mamhoodi and Gallant, 2021) and experimental (Okamura et al., 2006; Yegian et al.,

530 2007; Eseller-Bayat et al., 2013) tests reported in the literature.

531

4. Laboratory measurement of true SWRC and air-discontinuity point

The analytical and numerical modelling results presented above show that, once air trapping commences, the apparent SWRC measured in a wetting test will depend upon many aspects of the wetting test conditions, including: the dimensions of the soil sample; the method of suction application; the precise sequence of values of externally applied suction; and the time duration used for the application of each value of external suction. Hence, the apparent SWRC is the result of a particular boundary value problem (the wetting test on the soil sample), rather than a fundamental representation of the soil behaviour, and it is not applicable to any other boundary value problem. This means that an apparent SWRC from a laboratory test that is affected by air trapping should not be used directly in numerical modelling of other boundary value problems. The only correct way to represent the occurrence and influence of air trapping during wetting in numerical modelling of boundary value problems is to use the true SWRC in combination with a gas conductivity expression that goes to zero at the air-discontinuity point (such as Equation 8). This means that it is important to be able to determine by laboratory testing both the true SWRC and the air-discontinuity value of degree of saturation $S_{l,AD}$.

The numerical modelling results presented above demonstrate that laboratory measurement of a true wetting SWRC over the full range of degree of saturation is feasible for clays, because, in wetting tests on clays, diffusion of dissolved air occurs over a timescale that means it is realistic to wait until diffusion has fully dissipated excess gas pressure within any trapped air for each decrement of externally applied suction. It is, however, important, in order to achieve this dissipation of excess gas pressure within trapped air, to use appropriate timescales for each stage (e.g. of the order of 600 hours for a sample 20mm high) for the final wetting stages at high values of S_l, rather than assuming it is acceptable to reduce the time duration for stages at high values of S_l because of the high liquid conductivity.

In contrast, the numerical modelling results presented above suggest that laboratory measurement of a true wetting SWRC over the full range of degree of saturation is likely to be problematic for sands, because, once air trapping occurs, the timescales required for full dissipation of excess gas pressure in trapped air by diffusion of dissolved air are likely to be

562 impractical (well in excess of 600 hours for each stage for a sample 20mm high). Given that

563 laboratory measurement of the final part of the true SWRC for a main wetting curve (at high values

564 of S_l) may not be feasible in sands, because of the excessive timescales required once air

565 trapping occurs, it may be best to simply infer a shape for the final part of the curve, based on

566 reliable measurements for the rest of the main wetting SWRC (before air trapping occurs).

567 Information on the shape of the main drying curve at high values of S_l may also be useful. For

568 example, it might be assumed that the form of the main wetting curve at high values of S_l is simply

569 given by a horizontal translation of the main drying curve in the standard semi-logarithmic plot of

570 S_l against s.

571

572 As mentioned above, the degree of saturation at the air discontinuity point $S_{l,AD}$ is typically in the

573 range of 0.85 ± 0.1 (Likos et al, 2013). In order to determine a specific value of $S_{l,AD}$ for a particular

574 soil by laboratory testing, it would be desirable to devise a wetting test procedure where air

575 trapping occurs and the value of $S_{l,AD}$ is very clear from the shape of the apparent SWRC. Ideal

576 examples are the dotted curves in Figure 1, representing apparent SWRCs for an infinitesimal

577 element if diffusion of dissolved air is excluded and suction is applied by varying $p_{g,ext}$ with $p_{l,ext}$

578 maintained constant. In these idealised curves, for an infinitesimal element with diffusion

579 excluded, the value of $S_{l,AD}$ can be precisely identified. The challenge is to try to devise a practical

580 laboratory test procedure, for use on real soil samples of finite size, that produces apparent

581 SWRCs as similar as possible to these idealised curves.

582

583 The proposed laboratory test procedure for determination of the value of $S_{l,AD}$ is as follows:

584   1) A wetting SWRC test is performed by decreasing the external pore-gas pressure $p_{g,ext}$

585   while maintaining the external liquid pressure $p_{l,ext}$ constant. In this way, changes in

586   degree of saturation due to compression of trapped air are prevented.

587   2) When a relatively high value of the average degree of saturation is attained during the

588   test, i.e. about $\bar{S}_l = 0.7$, further decreases of the externally applied suction are applied by

589   means of very small steps. This prevents situations in which trapped air is formed at the

590   boundary while the remainder of the specimen is at much lower degree of saturation,

591   leading to a final average degree of saturation $\overline{S}_l$ much lower than $S_{l,AD}$ (e.g. path 2 in

592   Figure 5).

593   3) The time interval of each small suction step must be no longer than the time sufficient to

594   achieve equalisation of gas and liquid pressures within the sample, in order to limit the

595   effect of diffusion of dissolved air.

596   4) The test can be concluded using larger suction step decreases once the apparent wetting

597   SWRC exhibits a sub-horizontal trend. This final degree of saturation value can be taken

598   as the degree of saturation at the air-discontinuity point $S_{l,AD}$.

599

600   This procedure was simulated numerically on the sand sample, with diffusion of dissolved air

601   included. The apparent SWRC obtained with this procedure is shown in Figure 10, where it is

602   compared with the true SWRC. After an initial suction step from 10 kPa to 3 kPa with a time

603   duration of 2 hours, suction was further decreased by steps of 0.1 kPa. The time interval for each

604   step was adjusted such that it was just sufficient to achieve equalisation of gas and liquid

605   pressure, but with a maximum time interval of 2 hours, corresponding to the time interval used for

606   the suction steps for low and medium degree of saturation values. After the apparent SWRC

607   showed a constant value of $\overline{S}_l$, the test was concluded by applying $s_{ext} = 0$. The apparent SWRC

608   obtained with this simulation showed a clear horizontal trend for values of suction lower than 2

609   kPa. This defined an apparent degree of saturation value at the air-discontinuity point of

610   approximately 0.84, which was very close to $S_{l,AD} = 0.85$, which was the actual value used to

611   model the hydraulic behaviour of the sand.

612

613   This proposed method for laboratory determination of $S_{l,AD}$ has however some limitations. The

614   accuracy of the determination of $S_{l,AD}$ depends on the resolution of the suction step changes

615   adopted in proximity of the air-discontinuity point. Moreover, the method cannot be reliably applied

616   to fine-grained soils where numerical modelling showed it is difficult to find a time duration for

617   each wetting stage around the air discontinuity point that is sufficiently long to achieve full

618   equalisation of pore liquid pressure and pore gas pressure (at least until air trapping occurs) while

619   also being sufficiently short to ensure negligible impact of diffusion of dissolved air. It is notable,

620   that one of the main challenges arises because the time required for equalisation of pore gas

621   pressure by gas flow becomes very long in the last few small wetting steps before s_{ext} decreases

622   to the air-discontinuity value s_{AD}, because the relative gas conductivity k_{rg} becomes extremely

623   small when the suction is only slightly greater than s_{AD}.

624

625   Further research is required to develop laboratory procedures for determination of true wetting

626   SWRCs and air-discontinuity values of degree of saturation $S_{l,AD}$ that are practical and reliable for

627   all soils, noting that coarse-grained soils appear to be the most challenging when determining the

628   true SWRC and fine-grained soils appear to be the most challenging when determining the value

629   of $S_{l,AD}$.

630

631   **5. Conclusions**

632   At high values of degree of liquid saturation S_l, the apparent soil water retention curve (SWRC)

633   measured in a wetting test in the laboratory (S_l plotted against the externally applied suction s_{ext})

634   may differ from the true SWRC (S_l plotted against the internal suction s within the soil sample).

635   This is because of the occurrence of air trapping within the soil, when the gas phase becomes

636   discontinuous, and the fact that the gas pressure within the trapped air will then be higher than

637   the externally applied gas pressure unless the very slow process of diffusion of dissolved air has

638   finished. Due to the occurrence of air trapping, the apparent SWRC will typically not reach a fully

639   saturated condition as the externally applied suction s_{ext} is reduced to zero. In contrast, physical

640   arguments indicate that, with the exception of hydrophobic soils, the true SWRC will reach full

641   saturation at a positive value of internal suction s.

642

643   Analytical modelling of air trapping within an infinitesimally small soil element (without any

644   diffusion of dissolved air) demonstrated how the apparent SWRC can differ from the true SWRC.

645   If wetting is produced by increasing the externally applied liquid pressure (rather than by

646   decreasing the externally applied gas pressure), this results in increases in the gas pressure

647   within the trapped air as s_{ext} is reduced towards zero, leading to compression of the trapped air

648   and hence increases of S_l after air trapping commences (even when diffusion of dissolved air is

649   excluded). The analytical modelling demonstrated that these increases of S_l after air trapping

650   commences will be much greater in a test on clay than in a test on sand, because higher values

651   of excess gas pressure within the trapped air are generated in a clay, as a consequence of the

652   fact that the air trapping commences at much higher values of suction in a clay than in a sand.

653   Conversely, if wetting is produced by decreasing the externally applied gas pressure, the gas

654   pressure within the trapped air remained constant after s_{ext} is reduced below the air-discontinuity

655   value s_{AD}, with no further changes of S_l after air trapping commences (when diffusion of dissolved

656   air is excluded). The analytical model of an infinitesimally small element with diffusion of dissolved

657   air excluded was able in its simplicity to capture key aspects of air trapping, which was

658   subsequently useful in the interpretation of numerical analyses of finite sized samples.

659

660   Numerical modelling of wetting tests on soil samples of finite size (involving simulations where

661   diffusion of dissolved air was included and simulations where this diffusion was excluded) showed

662   that, once air trapping commences, the apparent SWRC measured in a wetting test will depend

663   upon many aspects of the wetting test conditions. These include: the method of suction

664   application (whether wetting is produced by increasing the externally applied liquid pressure or

665   by decreasing the externally applied gas pressure); the precise sequence of values of externally

666   applied suction; and the time duration used for the application of each value of external suction.

667   Hence, the apparent SWRC is the result of a particular boundary value problem (the wetting test

668   on the soil sample), rather than a fundamental representation of the soil behaviour. In contrast,

669   the true SWRC is a fundamental representation of the soil behaviour.

670

671   Given that the apparent SWRC measured in a wetting test in a laboratory applies only to the

672   specific boundary value problem of this laboratory test, this apparent SWRC is not applicable to

673   any other boundary value problem. Hence, the apparent SWRC from the laboratory test should

674   not be used in numerical modelling of other boundary value problems. The only correct way to

675   represent the occurrence and influence of air trapping during wetting in numerical modelling of

676   boundary value problems is to use the true SWRC in combination with a gas conductivity

677   expression that goes to zero at the air-discontinuity point. This was demonstrated in the numerical

678   modelling of finite sized samples presented in this paper, but it would also apply to numerical

679   modelling of larger scale boundary value problems.

680

681   Air trapping is one of the main causes of water retention hysteresis. As such, correct

682   understanding of the phenomenon of air trapping is crucial for appropriate interpretation of water

683   retention hysteresis data including trapped air (e.g. Wen et al., 2020) and the calibration of water

684   retention constitutive models (e.g. Dias et al., 2021) for use in numerical analyses. Appropriate

685   understanding of the true values of the pore gas and liquid pressures, and hence suction, is also

686   significant for the representation of mechanical behaviour by unsaturated mechanical constitutive

687   models (e.g. Alonso et al., 1990) within coupled hydro-mechanical numerical modelling or for

688   prediction of unsaturated shear strength (e.g. Albadri et al., 2021) for use in stability analyses.

689

690   Further research is required to devise appropriate experimental procedures, suitable for all soils,

691   for determination of true wetting SWRCs within the range of S_l where air trapping occurs and to

692   measure the degree of saturation corresponding to the air-discontinuity point $S_{l,AD}$. This might be

693   facilitated by use of advanced visualisation techniques, such as X-ray computed tomography,

694   capable of providing insights into the distribution of trapped air within soils (e.g. Kido et al, 2020).

695   Accurate determination of the true wetting SWRC in the range where air trapping occurs is most

696   demanding for coarse-grained soils, because diffusion of dissolved air is exceptionally slow in

697   coarse-grained soils. In contrast, initial studies indicate that accurate determination of the value

698   of $S_{l,AD}$ is most demanding for fine-grained soils, because, at values of S_l approaching $S_{l,AD}$, the

699   timescale required for equalisation of pore gas pressure and the timescale required for diffusion

700   of dissolved air are similar.

701

702   **References**

703   Albadri WM, Noor MJM & Alhani IJ (2021). The relationship between the shear strength and water

704   retention curve of unsaturated sand at different hydraulic phases. *Acta Geotechnica*, 1-15.

705   Alonso EE, Gens A and Josa A (1990). A constitutive model for partially saturated soils.

706   *Géotechnique*, 40(3), 405-430.

707   Beriozkin A and Mualem Y (2018). Comparative analysis of the apparent saturation hysteresis

708   approach and the domain theory of hysteresis in respect of prediction of scanning curves and

709   air entrapment. *Advances in Water Resources*, 115: 253-263.

710 Brooks RH and Corey TA (1964). Hydraulic properties of porous media. Hydrology Paper No.3,

711   Civil Engineering Department, Colorado State University, Fort Collins, CO.

712 Chen P and Wei C (2016). Numerical procedure for simulating the two-phase flow in unsaturated

713   soils with hydraulic hysteresis. *International Journal of Geomechanics*, 16(1): 04015030.

714 Chen P, Wei C and Ma T (2015). Analytical model of soil-water characteristics considering the

715   effect of air entrapment. International Journal of Geomechanics 15(6): 04014102.

716 Chen P, Lu N and Wei C (2019). General Scanning Hysteresis Model for Soil–Water Retention

717   Curves. *Journal of Geotechnical and Geoenvironmental Engineering*, 145(12): 04019116.

718 Dias AS, Pirone M, Nicotera MV & Urciuoli G (2021). Hydraulic hysteresis of natural pyroclastic

719   soils in partially saturated conditions: experimental investigation and modelling. *Acta

720   Geotechnica*, 1-19.

721 Eseller-Bayat E, Yegian MK, Alshawabkeh A and Gokyer S (2013). Liquefaction response of

722   partially saturated sands. II: Empirical model. *Journal of Geotechnical and Geoenvironmental

723   Engineering*. 139 (6): 872–879.

724 Fayer MJ and Hillel D (1986a). Air encapsulation: I. Measurement in a field soil. *Soil Science

725   Society of America Journal*, 50(3): 568-572.

726 Fayer MJ and Hillel D (1986b). Air encapsulation: II. Profile water storage and shallow water table

727   fluctuations. *Soil Science Society of America Journal*, 50(3): 572-577.

728 Fischer U, Dury O, Flühler H and van Genuchten MT (1997). Modeling nonwetting-phase relative

729   permeability accounting for a discontinuous nonwetting phase. *Soil Science Society of

730   America Journal*, 61(5): 1348-1354.

731 Haines, WB (1930). The hysteresis effect in capillary properties and the modes of moisture

732   distribution associated therewith. *The Journal of Agricultural Science*, 20: 96–105.

733 Hannes M, Wollschläger U, Wöhling T and Vogel HJ (2016). Revisiting hydraulic hysteresis based

734   on long-term monitoring of hydraulic states in lysimeters. *Water Resources Research*, 52(5):

735   3847-3865.

736 Hilf JW (1956). An investigation of pore-water pressure in compacted cohesive soils, Ph. D.

737   Thesis. Technical Memorandum No. 654, United State Department of the Interior Bureau of

738   Reclamation, Design and Construction Division, Denver, Colorado, USA.

739 Kido R, Higo Y, Takamura F, Morishita R, Khaddour G & Salager S (2020). Morphological

740   transitions for pore water and pore air during drying and wetting processes in partially

741   saturated sand. *Acta Geotechnica*, 15: 1745-1761.

742 Killough JE (1976). Reservoir simulation with history-dependent saturation functions. *Society of

743   Petroleum Engineers Journal*, 16(01): 37-48.

744 Kool JB and Parker JC (1987). Development and evaluation of closed-form expressions for

745   hysteretic soil hydraulic properties. *Water Resources Research*, 23(1): 105-114.

746 Likos WJ, Lu N and Godt JW (2013). Hysteresis and uncertainty in soil water-retention curve

747   parameters. *Journal of Geotechnical and Geoenvironmental Engineering*, 140(4): 04013050.

748 Mahmoodi B and Gallant A (2021). Assessing Persistence of Entrapped Gas for Induced Partial

749   Saturation. *Journal of Geotechnical and Geoenvironmental Engineering*, 147(3): 04020184.

750 Millington RJ and Quirk JP (1961). Permeability of porous solids. *Transactions of the Faraday

751   Society*, 57: 1200-1207.

752 Mualem Y (1976). A new model for predicting the hydraulic conductivity of unsaturated porous

753   media. *Water resources research*, 12(3): 513-522.

754 Okamura M, Ishihara M and Tamura K (2006). Degree of saturation and liquefaction resistances

755   of sand improved with sand compaction pile. *Journal of Geotechnical and Geoenvironmental

756   Engineering*, 132 (2): 258–264.

757 Olivella S, Gens A, Carrera J and Alonso EE (1996). Numerical formulation for a simulator

758   (CODE_BRIGHT) for the coupled analysis of saline media. *Engineering computations*, 13(7):

759   87-112.

760 Peck AJ (1960). Change of moisture tension with temperature and air pressure: Theoretical. *Soil

761   Science*, 89(6): 303-310.

762 Pham HQ, Fredlund DG and Barbour SL (2005). A study of hysteresis models for soil-water

763   characteristic curves. *Canadian Geotechnical Journal*, 42(6): 1548-1568.

764 Poulovassilis A (1970). The effect of the entrapped air on the hysteresis curves of a porous body

765   and on its hydraulic conductivity. *Soil Science*, 109(3): 154-162.

766 Richards LA and Fireman M (1943). Pressure-plate apparatus for measuring moisture sorption

767   and transmission by soils. *Soil Science*, 56(6): 395-404.

768 Scarfone R (2020). Modelling the hydraulic behaviour of unsaturated soils and application to the

769   numerical and experimental study of capillary barrier systems. PhD thesis, University of

770   Glasgow.

771 Scarfone R, Wheeler SJ and Lloret-Cabot M (2020). Conceptual hydraulic conductivity model for

772   unsaturated soils at low degree of saturation and its application to the study of capillary barrier

773   systems. *Journal of Geotechnical and Geoenvironmental Engineering*, *146*(10), 04020106.

774 Sharma RS and Mohamed MH (2003). An experimental investigation of LNAPL migration in an

775   unsaturated/saturated sand. *Engineering Geology*, 70(3-4): 305-313.

776 Stonestrom DA and Rubin J (1989). Water content dependence of trapped air in two soils. *Water

777   Resources Research*, 25(9): 1947-1958.

778 van Geel PJ and Sykes JF (1997). The importance of fluid entrapment, saturation hysteresis and

779   residual saturations on the distribution of a lighter-than-water non-aqueous phase liquid in a

780   variably saturated sand medium. *Journal of Contaminant Hydrology*, 25(3-4): 249-270.

781 van Genuchten MT (1980). A closed-form equation for predicting the hydraulic conductivity of

782   unsaturated soils 1. *Soil science society of America journal*, 44(5): 892-898.

783 Wen T, Shao L, Guo X & Zhao Y (2020). Experimental investigations of the soil water retention

784   curve under multiple drying–wetting cycles. *Acta Geotechnica*, 15(11): 3321-3326.

785 Williams PJ (1966). Movement of air through water in partly saturated soils. *Nature*, 212(5069):

786   1463.

787 Yegian MK, Eseller-Bayat E, Alshawabkeh AS and Ali S (2007). Induced-partial saturation for

788   liquefaction mitigation: experimental investigation. *Journal of geotechnical and
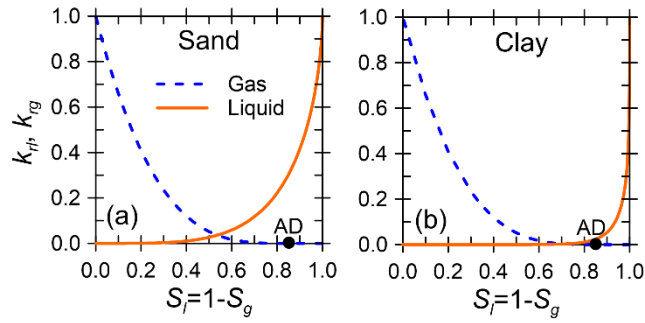
789   geoenvironmental engineering*, 133(4): 372-380.

Figures.
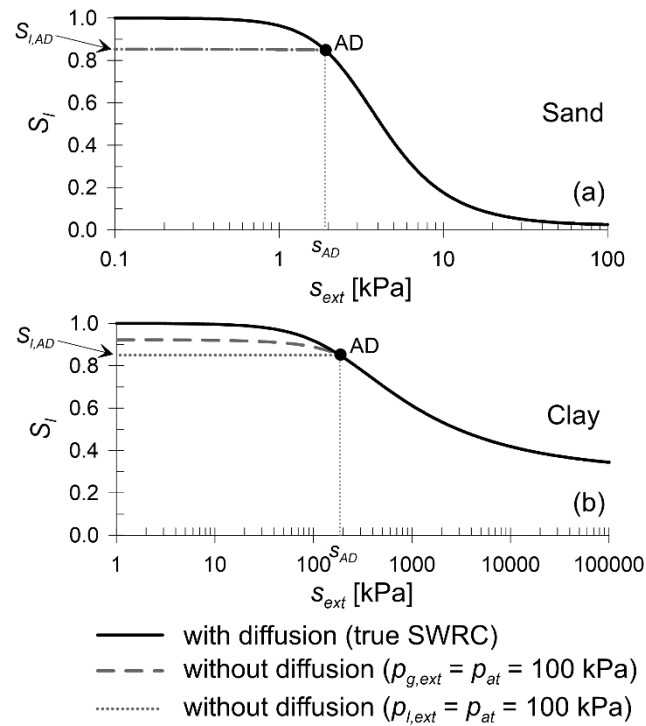
Fig. 1. Apparent SWRC for infinitesimal element with and without diffusion of dissolved air for (a) sand and (b) clay
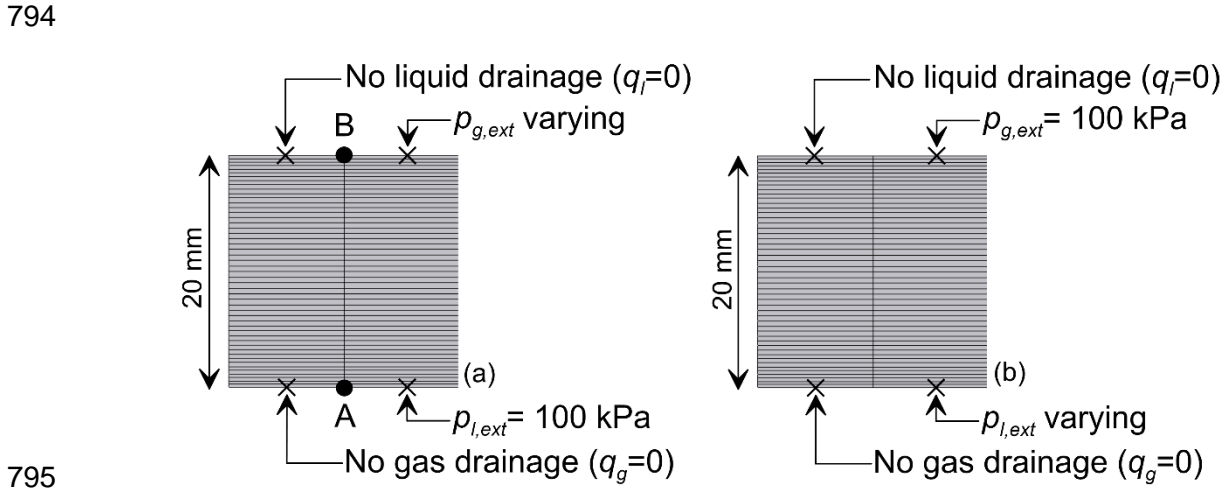
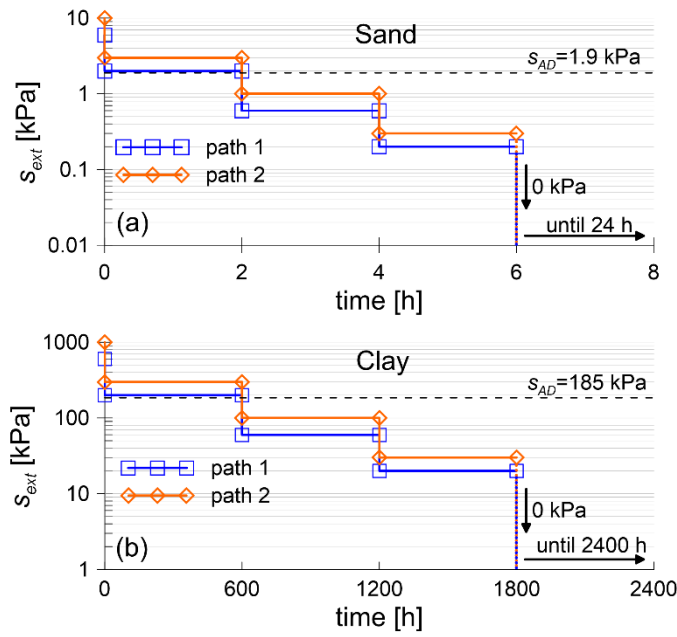**Fig. 2.** Numerical models

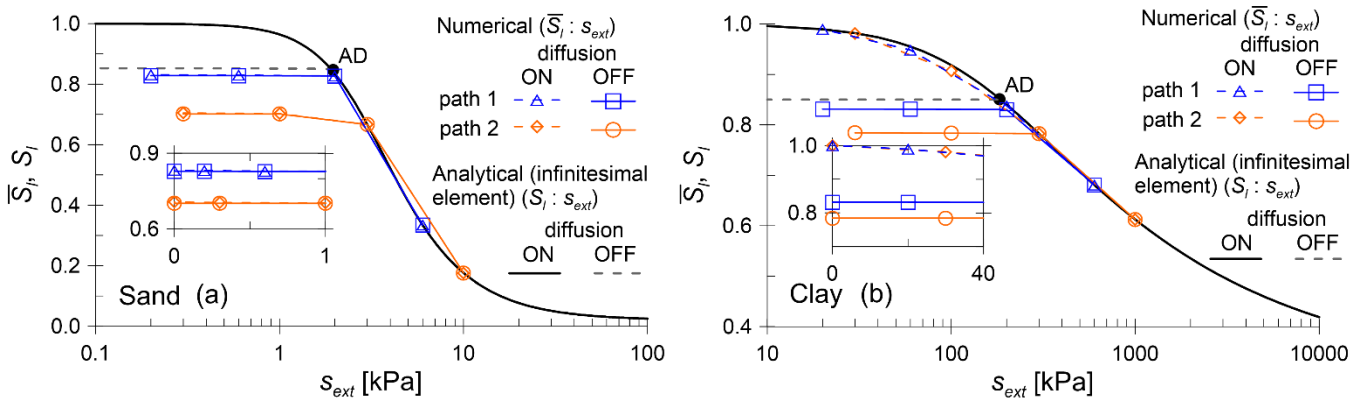**Fig. 3.** Relative liquid conductivity k_{rl} and relative gas conductivity k_{rg} plotted against degree of liquid saturation S_l, for (a) sand and (b) clay
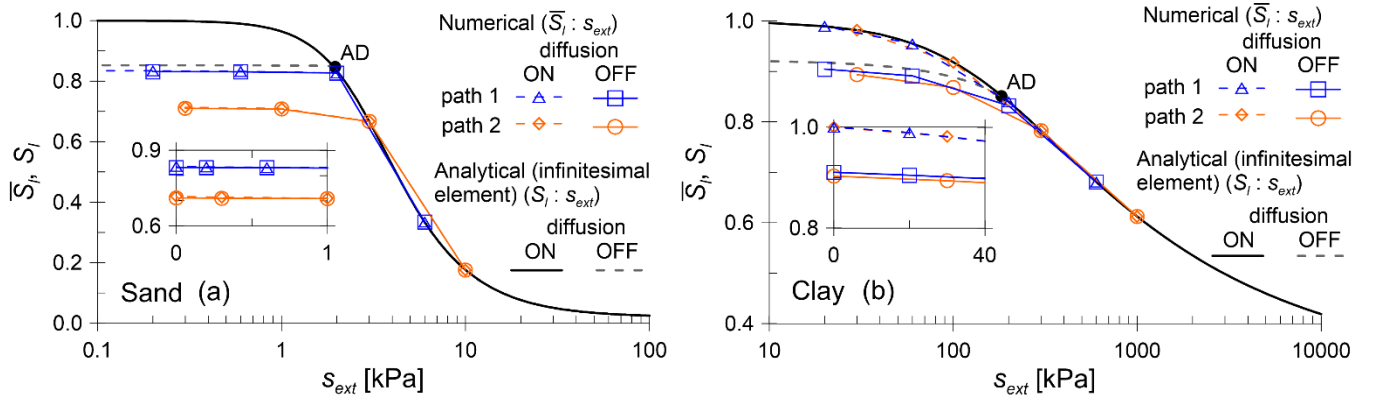

Fig. 4. Time history of externally applied suction s_{ext} for (a) sand and (b) clay

Fig. 5. Apparent SWRCs, obtained from the numerical analyses with $p_{l,ext}$ = 100 kPa for (a) sand and (b) clay, compared against equivalent analytical results for an infinitesimal element

Fig. 6. Apparent SWRCs, obtained from the numerical analyses with $p_{g,ext}$ = 100 kPa for (a) sand and (b) clay, compared against equivalent analytical results for an infinitesimal element
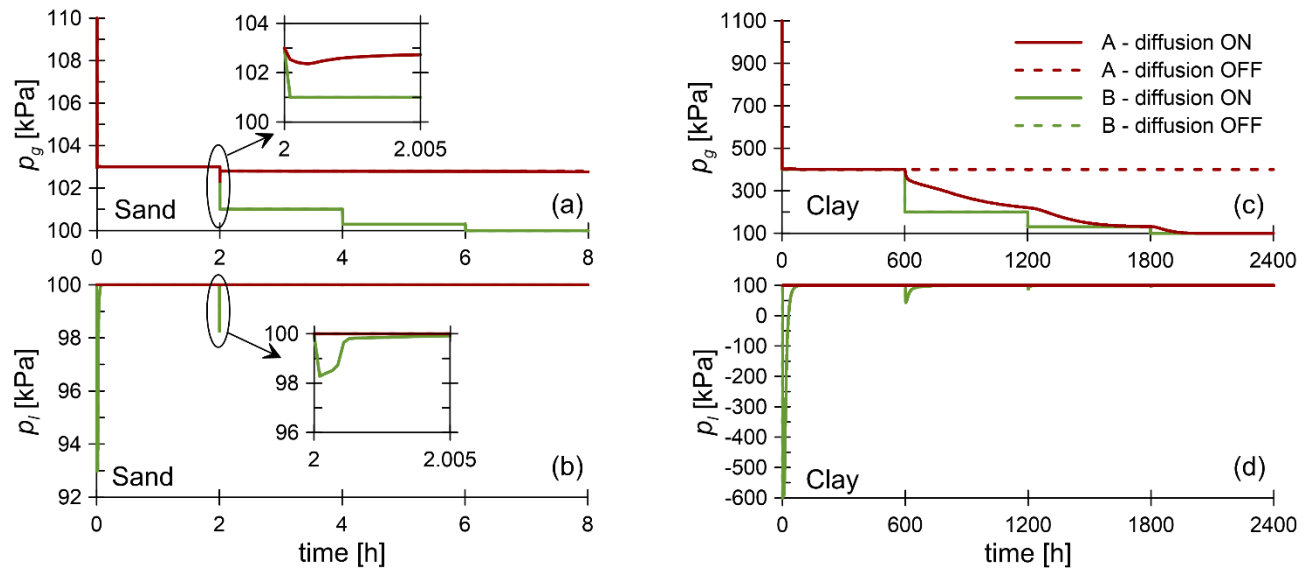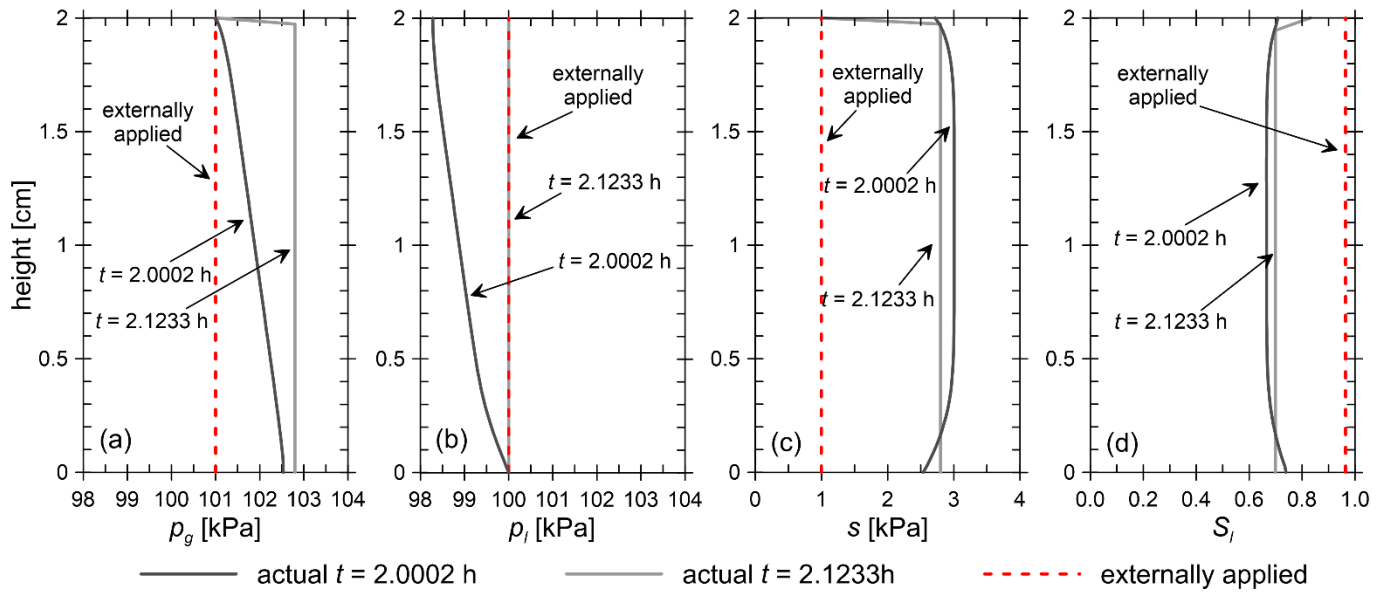
Fig. 7. Time histories of liquid pressure p_l and gas pressure p_g at positions A and B, for path 2 applied to (a-b) sand and (c-d) clay, with $p_{l,ext}$ = 100 kPa.
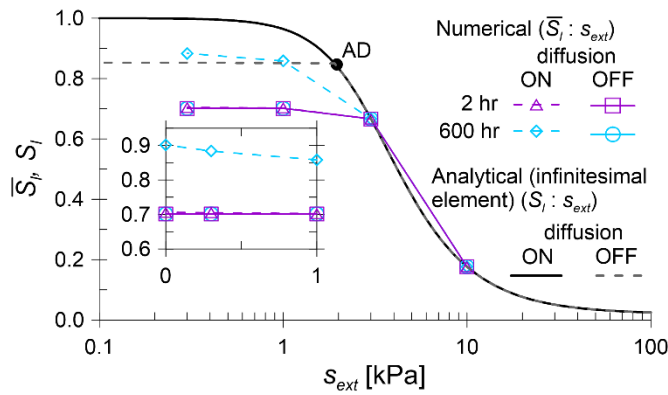
819

Fig. 8. Profiles of (a) pore gas pressure, (b) pore liquid pressure, (c) suction and (d) degree
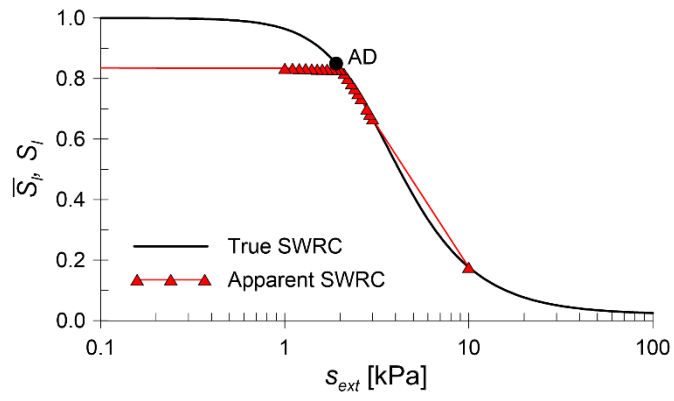of saturation within the sand sample for path 2, with $p_{l,ext}$ = 100 kPa.

825

Fig. 9. Apparent SWRCs: influence of the time duration of each value of applied suction, for
path 2 applied to sand with $p_{l,ext}$ =100 kPa.

828

829

830 **Fig. 10.** Results of the simulation of a SWRC test aimed to determine the air-discontinuity
831 point of the sand

832

833

834 **Tables.**

835 Table 1. Constitutive laws and parameters used for the materials in the analytical model (only SWRC)

836 and in the numerical models

Constitutive law		Parameters	
Soil water retention curve SWRC – van Genuchten (1980)	$S_e = \dfrac{S_l - S_{rl}}{S_{ls} - S_{rl}} = \left[1 + \left(\dfrac{p_g - p_l}{P_0} \right)^{\frac{1}{1-\lambda}} \right]^{-\lambda}$	Sand	$\lambda = 0.6$, $P_o = 0.003$ MPa, $S_{rl} = 0.02$, $S_{ls} = 1$
		Clay	$\lambda = 0.3$, $P_o = 0.160$ MPa, $S_{rl} = 0.3$, $S_{ls} = 1$
Relative hydraulic conductivity – Mualem (1976)	$k_{rl} = \sqrt{S_e} \left[1 - \left(1 - S_e^{1/\lambda} \right)^{\lambda} \right]^2$		
Relative gas conductivity	$k_{rg} = A S_{eg}^n, \qquad S_{eg} = \dfrac{S_g - S_{rg}}{S_{gs} - S_{rg}}$	Sand & Clay	$A = 1$, $n = 3.333$, $S_{rg} = 0.15$, $S_{gs} = 1$
Intrinsic permeability for Darcy's Law	$q_\alpha = -\dfrac{k k_{r\alpha}}{\mu_\alpha} (\nabla p_\alpha - \rho_\alpha g)$	Sand	$k = 3\text{x}10^{-12}$ m^2
		Clay	$k = 1\text{x}10^{-16}$ m^2
Diffusive flux of air in the liquid phase (Fick's Law)	$i_l^a = -\left(\tau \phi \rho_l S_l D_l^a \mathbf{I} \right) \nabla \omega_l^a$ $D_l^a = D \exp\left(\dfrac{-Q}{R(273.15 + T)} \right)$	Sand	$\phi = 0.40$, $\tau = 1$, $D = 1.1\text{x}10^{-4}$ m^2/s, $Q = 24530$ J/mol
		Clay	$\phi = 0.38$, $\tau = 1$, $D = 1.1\text{x}10^{-4}$ m^2/s, $Q = 24530$ J/mol
Concentration of air in the liquid phase (Henry's Law)	$\omega_l^a = \dfrac{p_a}{H} \dfrac{M_a}{M_w}$		
Liquid viscosity	$\mu_l = A \exp\left(\dfrac{B}{273.15 + T} \right)$	Sand & Clay	$A = 2.1\text{x}10^{-12}$ MPa·s, $B = 1808.5$K
Gas viscosity	$\mu_l = \dfrac{A\sqrt{273.15 + T}}{\left(1 + \dfrac{B}{273.15 + T} \right)} \dfrac{1}{1 + \dfrac{b_k}{p_g}}$, $b_k = C - Dk$	Sand & Clay	$A = 1.48\text{x}10^{-12}$ MPa·s, $B = 392.55$ K, $C = 0.14$ MPa, $D = 1.2\text{x}10^{15}$ MPa·m^{-2}

837 S_l = (liquid) degree of saturation, S_e = effective (liquid) degree of saturation, S_{rl} = residual degree of saturation, S_{ls} = maximum
838 degree of saturation, k_{rl} = relative hydraulic conductivity, k_{rg} = relative gas conductivity, S_g = gas degree of saturation expressed
839 as $S_g = 1 - S_l$, S_{ge} = effective gas degree of saturation, S_{rg} = residual gas degree of saturation, S_{gs} = maximum gas degree of
840 saturation, q_α = advective flow rate (m/s) of phase α where α = l for liquid and α = g for gas, k = intrinsic permeability (m^2), μ_α =
841 viscosity of phase α (MPa·s), ρ_α = density of phase α (kg/m^3), g = gravity (set to 0 m/s^2 for simplicity), i_l^a = diffusive flow of air in
842 the liquid phase (kg·m^{-3}·s^{-1}), τ = tortuosity, ϕ = porosity, D_l^a = diffusion coefficient of air in the liquid phase (m^2/s), ω_l^a = air mass
843 fraction in the liquid phase (kg of air per m^3 of liquid), R = ideal gas constant (8.3143 J/mol/K), T = temperature (°C) (constant
844 and uniform at 20°C), p_a = dry air pressure (MPa), H = Henry's constant (10000 MPa), M_a = molecular mass of dry air, M_w =
845 molecular mass of water.
846